Liver Research 9 (2025) 132–143

Contents lists available at ScienceDirect

Liver Research

journal homepage: http://www.keaipublishing.com/en/journals/liver-research

Original Article

Anti-PD-1 synergizes with RFA to suppress abscopal tumors and induce durable memory against recurrence in HCC

Kai Lei [a, 1], Shuang Li [a, 1], Jiale Chen [b, 1], Zebin Chen [a, *], Fang Wang [c, **], Xuezhen Zeng [a, d, ***]

[a] Department of Liver Surgery, Center of Hepato-Pancreato-Biliary Surgery, The First Affiliated Hospital, Sun Yat-sen University, Guangzhou, Guangdong, China
[b] Department of Gastroenterology and Hepatology, The First Affiliated Hospital, Sun Yat-sen University, Guangzhou, Guangdong, China
[c] Department of Oncology, The First Affiliated Hospital, Sun Yat-sen University, Guangzhou, Guangdong, China
[d] Institute of Precision Medicine, The First Affiliated Hospital, Sun Yat-sen University, Guangzhou, Guangdong, China

ARTICLE INFO

Article history:
Received 1 April 2025
Received in revised form
16 April 2025
Accepted 15 May 2025

Keywords:
Radiofrequency ablation (RFA)
Hepatocellular carcinoma (HCC)
Abscopal effect
Anti-programmed cell death protein 1 (αPD-1)

ABSTRACT

Background and aims: Radiofrequency ablation (RFA) is the first-line treatment for early-stage hepatocellular carcinoma (HCC). However, recurrence after curative RFA remains a significant challenge for HCC patients. Although RFA induces an immune response, the anti-tumor effect is often limited by the immunosuppressive tumor microenvironment. Enhancing anti-tumor immunity is essential to improve treatment efficacy and prevent recurrence. In this study, we explore the efficacy and underlying mechanisms of the combination of RFA and anti-PD-1 in suppressing abscopal and recurrent tumors.

Methods: We established a bilateral subcutaneous HCC mouse model and performed complete RFA on the right-flank tumor. Anti-PD-1 or anti-IgG was administered post-RFA. Tumor growth, immune cell profiles, and molecular pathways were assessed using flow cytometry, immunohistochemistry staining, RNA-sequencing, and Western blot. Chemokines released by the tumor were detected by ELISA. An *in vivo* tumor rechallenge experiment was performed after a complete tumor regression to evaluate the immune memory induced by the RFA+anti-PD-1 treatment.

Results: RFA combined with anti-PD-1 significantly suppressed abscopal tumor growth and prolonged survival. Compared with RFA monotherapy, the infiltration of $CD8^+$T cells and dendritic cells was significantly increased in the combined treatment group, while PMN-MDSCs were markedly reduced. Mechanistically, the chemokine signaling pathway and JAK-STAT signaling pathway were activated in the tumor of the RFA+anti-PD-1 group with upregulation of CXCL10 to recruit $CD8^+$T cells. In addition, the combination therapy induced durable immune memory that inhibited rechallenge tumor outgrowth.

Conclusions: Our study discovered that RFA combined with anti-PD-1 induced anti-tumor immunity to inhibit abscopal tumors and durable immune memory to prevent recurrence, suggesting RFA+anti-PD-1 as a potential therapeutic strategy for multifocal HCC and preventing recurrence.

1. Introduction

Hepatocellular carcinoma (HCC) is the most common type of primary liver cancer and ranks as the fourth leading cause of cancer-related death globally.[1,2] Radiofrequency ablation (RFA) is the first-line curative treatment modality and is widely used for HCC.[1,3] RFA, a minimally invasive modality, utilizes high-frequency electrical currents to generate localized hyperthermia, inducing protein denaturation and coagulative necrosis of tumor cells.[4] The destruction of the tumor releases a large amount of tumor-specific

* Corresponding author.
** Corresponding author.
*** Corresponding author. Department of Liver Surgery; Institute of Precision Medicine, The First Affiliated Hospital, Sun Yat-sen University, Guangzhou, Guangdong, China.
E-mail addresses: chenzb23@mail.sysu.edu.cn (Zebin Chen), wangf72@mail.sysu.edu.cn (Fang Wang), zengxzh7@mail.sysu.edu.cn (Xuezhen Zeng).
Peer review under the responsibility of Editorial Office of Liver Research.
[1] These authors contributed equally to this study.

https://doi.org/10.1016/j.livres.2025.05.003

antigen (TSA), which triggers anti-tumor immunity.[5–9] Accumulating studies have demonstrated that RFA increases the production of proinflammatory cytokines, which recruit dendritic cells (DCs) and plasma cells, further enhancing anti-tumor immune response.[8,9]

In addition to the eradication of local tumors, increasing evidence shows that tumor ablation can also induce spontaneous distant tumor regression, which is known as the abscopal effect.[10,11] Previous studies have shown that the ablation of a unilateral tumor can significantly inhibit the growth of distant tumors in pancreatic ductal adenocarcinoma (PDAC) and HCC.[6,12] However, in clinical practice, the anti-tumor immune response induced by RFA is insufficient to completely prevent HCC recurrence.[5] Moreover, incomplete ablation of tumor lesions can reshape the immunosuppressive microenvironment to inhibit anti-tumor immunity and promote tumor recurrence.[6,12] Another study reported that RFA upregulated the expression of programmed cell death protein-1 (PD-1) and lymphocyte activation gene 3 (LAG-3) in distant tumors, which suppressed anti-tumor immunity and caused rapid tumor regrowth.[13] These studies suggest that adjuvant therapy is needed to boost anti-tumor immunity and enhance the abscopal effect of RFA.

Immune checkpoint inhibitors (ICIs) have revolutionized cancer treatment. Targeting PD-1 or its ligand PD-L1 can rescue T cells from exhaustion and restore immune responses against cancer cells.[14] Previous studies suggest that RFA and anti-PD-1 (αPD-1). treatment can effectively eliminate primary tumors and enhance the abscopal effect.[15] The observed effect depends on $CD8^+$ T cells, but further investigation is needed to fully understand how RFA combined with PD-1 therapy affects tumor progression at distant sites.

In this study, we aimed to investigate whether combining RFA with αPD-1 therapy could enhance the abscopal effect and improve survival in a bilateral murine HCC model. We also explored the underlying mechanisms by which this combination strategy enhances anti-tumor immunity, with a focus on $CD8^+$T cells and cytokine-mediated signaling pathways.

2. Materials and methods

2.1. Ethics approval

All animal procedures in this study were approved by the Institutional Animal Care and Use Committee (IACUC) of Sun Yat-sen University (approval No. SYSU-IACUC-2023-000249) and conducted in accordance with the ARRIVE guidelines and international ethical standards. During the experiment, all animal care and procedures adhered to humane principles, minimizing animal suffering and discomfort to the greatest extent possible.

2.2. Animal experiment

Male C57BL/6J mice (6–8 weeks old) were purchased from GemPharmatech Co., Ltd. (Nanjing, China) and were maintained under specific pathogen-free conditions with a 12-h light/dark cycle, at a temperature of ~18–23 °C, and air humidity of 40%–60% in the animal facility of the Animal Experiment Center of Sun Yat-sen University.

Hepa 1–6 cells (5×10^6 cells) in 200 μL phosphate-buffered saline (PBS) solution were subcutaneously injected into both the left and right flanks of the mice. Tumor growth was monitored using caliper measurements. All mice underwent RFA treatment 14 days after tumor implantation, when the tumor volume reached 500 mm^3. All mice were randomly divided into two groups using a computer-generated randomization sequence with stratification by initial tumor volume and body weight: RFA ($n = 7$) and RFA+αPD-1 ($n = 10$). The allocation ratio was adjusted based on preliminary data indicating that RFA+αPD-1 induced complete regression of abscopal tumors in 85% of mice (versus 0% in RFA alone). To ensure adequate abscopal tumor samples for downstream analyses (flow cytometry and immunohistochemistry (IHC) staining), we predetermined a minimum target of $n = 9$ for the combination group while maintaining randomization integrity through blinded allocation procedures. For survival analysis, we performed the same experiments, and the number of mice was 16 for each group. Survival time was recorded from the day of tumor implantation until euthanasia. Complete RFA was performed on the right-flank tumors of the mice, while the left-flank tumors remained untreated. After RFA treatment, 100 μg αPD-1 antibody (catalog number: RMP1-14; Bio X Cell, Lebanon, NH, USA) or 100 μg isotype-matched IgG antibody (catalog number: 2A3; Bio X Cell, Lebanon, NH, USA) were respectively peritoneally injected into the mice from RFA+αPD-1 or RFA group every five days for three doses. Tumor size was monitored and calculated with the formula: $\text{Volumes} = (\text{Length} \times \text{Width}^2)/2$.

After completing the experimental procedures, mice were euthanized in accordance with ethical guidelines by cervical dislocation under deep anesthesia induced by isoflurane, ensuring a quick and humane death.

For the rechallenge study, a total of 32 mice were used, with 16 mice in the RFA group and 16 mice in the RFA + αPD-1 group. For all procedures involving tumor implantation, RFA, and combination treatments, mice were anesthetized using isoflurane (Forene®; Abbott GmbH & Co. KG, Wiesbaden, Germany) via inhalation. Mice underwent RFA treatment 14 days after tumor implantation, when the tumor volume reached 500 mm^3. In the RFA group, mice were euthanized upon reaching humane endpoints, specifically when the tumor diameter exceeded 1500 mm or if signs of distress (*e.g.*, ulceration, impaired mobility, or weight loss >15%) were observed. In the RFA+αPD-1 group, mice with complete tumor regression—defined as no visible tumor and no palpable mass under the skin—underwent rechallenge 56 days after tumor inoculation. To perform the rechallenge experiment, these mice were inoculated with 5×10^6 Hepa 1–6 cells on the left flanks again. Tumor growth was monitored weekly, and peripheral blood was collected before and after tumor rechallenge for flow cytometry analysis. Twenty-five days after the rechallenge, all mice were sacrificed to collect blood for further analysis.

2.3. Cell culture

Hepa 1–6 cells, a murine HCC cell line, were obtained from the Cell Bank of the Chinese Academy of Sciences (Shanghai, China). The cells were cultured in Dulbecco's Modified Eagle Medium (DMEM; Gibco, Thermo Fisher Scientific, Waltham, MA, USA), supplemented with 10% fetal bovine serum (FBS; Gibco, Thermo Fisher Scientific, Waltham, MA, USA) and 1% penicillin-streptomycin. Cells were maintained at 37 °C in a humidified incubator with 5% CO_2. When cells reached approximately 80% confluency, they were harvested and resuspended in PBS (Gibco, Thermo Fisher Scientific, Waltham, MA, USA) for subsequent experiments.

2.4. Hematoxylin and eosin (H&E) staining

H&E staining was performed on tissue sections using a standard protocol. The tissues were cut into 4 μm sections. After deparaffinization in xylene, sections were rehydrated through a graded ethanol series (100%, 90%, and 80%). The tissue was then stained with Mayer's hematoxylin, followed by eosin. After eosin staining, the sections were dehydrated using 95% and 100% ethanol and

cleared in xylene. Finally, the slides were mounted with mounting medium and imaged using an automatic digital pathology slide scanner (model: KF-PRO-020; KFBIO, Ningbo, China).

2.5. IHC staining

After deparaffinization and rehydration of tissue sections, IHC staining was carried out. Endogenous peroxidase activity was blocked by incubating the sections in 3% hydrogen peroxide for 10 min. Antigen retrieval was performed using a pressure cooker at high pressure for 2.5 min. Once cooled, the sections were incubated with 20% goat serum at room temperature for 30 min to minimize nonspecific binding. Primary antibodies against CD8α (D4W2Z, 1:500; CST, Danvers, MA, USA), CD11b (EPR1344, 1:2000; Abcam, Cambridge, UK), lymphocyte antigen 6 complex locus G (Ly6G; E6Z1T, 1:200; CST, Danvers, MA, USA), and CD11c (EPR21826, 1:100; Abcam, Cambridge, UK) were applied overnight at 4 °C; the details are shown in Supplemental Table 1. After washing with PBS, the sections were incubated with a secondary antibody (Dako REAL EnVision/HRP, Rabbit/Mouse (ENV)) for 30 min at room temperature. The reaction was developed using a diaminobenzidine (DAB) chromogen kit (catalog number: K5007; Dako, Glostrup, Denmark), and counterstaining was performed with hematoxylin. The slides were mounted and visualized using an automatic digital pathology slide scanner (model: KF-PRO-020; KFBIO, Ningbo, China). ImageJ (version 1.54d; National Institutes of Health, Bethesda, Maryland, USA) was employed to determine the percentage of tumor-infiltrating immune cells.

2.6. Flow cytometry

Flow cytometry analysis was performed to evaluate immune cell populations. Single-cell suspensions were prepared by mechanically dissociating the tumors and spleen and filtering the cell mixture through a 70 μm mesh. To exclude dead cells, samples were stained with a fixable viability dye (FVS700; Cat# 564997; BD Biosciences, Franklin Lakes, NJ, USA) according to the manufacturer's protocol. The cells were washed with PBS containing 1% FBS and incubated with a blocking antibody (anti-Fc receptor) for 20 min at 4 °C to reduce nonspecific binding. The cells were then stained with fluorochrome-conjugated antibodies against CD45 (30-F11, BD Biosciences, Franklin Lakes, NJ, USA), CD11b (M1/70, BD Biosciences, Franklin Lakes, NJ, USA), CD11c (N418, BioLegend, San Diego, CA, USA), F4/80 (BM8, BioLegend, San Diego, CA, USA), Gr-1 (RB6-8C5, BD Biosciences, Franklin Lakes, NJ, USA), Ly6C (HK1.4, BioLegend, San Diego, CA, USA), Ly6G (1A8, Thermo Fisher Scientific, Waltham, MA, USA), CD3e (145-2C11, BD Biosciences, Franklin Lakes, NJ, USA), CD4 (GK1.5, BD Biosciences, Franklin Lakes, NJ, USA), CD8α (53−6.7, BioLegend, San Diego, CA, USA), CD19 (1D3, BD Biosciences, Franklin Lakes, NJ, USA), NK1.1 (PK136, BD Biosciences, Franklin Lakes, NJ, USA), CD62L (MEL-14, BD Biosciences, Franklin Lakes, NJ, USA), CD44 (IM7, BioLegend, San Diego, CA, USA) for 30 min at 4 °C in the dark. After staining, the cells were washed and resuspended in PBS containing 1% FBS, and flow cytometry was performed using a 5-laser flow cytometer (Aurora; Cytek Biosciences, Fremont, CA, USA). Data were analyzed with FlowJo software (version 10.8; BD Biosciences, Franklin Lakes, NJ, USA) to identify specific immune cell subsets based on fluorescence intensity. The antibodies used in this study are listed in Supplemental Table 2.

2.7. T cell proliferation assay

For the assessment of autologous T cell proliferation, $CD3^+CD8^+$T cells were isolated from the spleens of C57BL/6J mice and labeled with carboxyfluorescein succinimidyl ester (CFSE; 5 μmol/L; catalog number: c34554; Invitrogen, Carlsbad, CA, USA), and then co-cultured with $Ly6G^+$ polymorphonuclear myeloid-derived suppressor cells (PMN-MDSCs) that were isolated from abscopal tumors of RFA or RFA+αPD-1 group using an MDSC isolation kit (catalog number: 130-094-538; Miltenyi Biotec, Bergisch Gladbach, Germany). The co-culture was conducted in the presence of CD3/CD28 dynabeads (catalog number: 11452D; Invitrogen, Carlsbad, CA, USA) and recombinant interleukin-2 (IL-2; catalog number: 402-ML-100; R&D Systems, Minneapolis, MN, USA) for a duration of 5 days. T-cells with or without dynabead stimulation served as positive or negative controls, respectively. Flow cytometry was performed using a Cytek Aurora to obtain the surface staining for CD3/CD8 T cell markers and CFSE signals on T-cells. The percentage of proliferating cells was determined and analyzed using FlowJo software (version 10.8; BD Biosciences, Franklin Lakes, NJ, USA).

2.8. Pathway and gene set enrichment analysis

Differential gene expression analysis was performed using the R package "DESeq2" (v1.38.3). Raw read counts were imported into R and processed through the DESeq2 pipeline. Genes were considered differentially expressed if they met the thresholds of $|Log2FC| \geq 1$ and adjusted *P*-value (padj) < 0.05. Kyoto Encyclopedia of Genes and Genomes (KEGG) pathway enrichment analysis was performed using the R package "fgsea" (v1.24.0) to identify pathways enriched in specific gene lists. Pathways with an adjusted *P*-value<0.05 were deemed significantly enriched. Gene set enrichment analysis (GSEA) was carried out with the R package "clusterProfiler" using pathways from the KEGG database (https://www.kegg.jp/).

2.9. Quantitative polymerase chain reaction (qPCR)

qPCR was performed to assess the messenger RNA (mRNA) expression of target genes. Total RNA was extracted from tumor tissue samples using TRIzol reagent (catalog number: 15596018CN; Thermo Fisher Scientific, Waltham, MA, USA) and reverse transcribed into complementary DNA (cDNA) using the PrimeScript RT Master Mix Kit (catalog number: RR036A; Takara Bio, Shiga, Japan). cDNA was then amplified using specific primers for the target genes. Gene expression levels were normalized to *Gapdh*, and relative expression was calculated using the ΔΔCt method. Three independent biological replicates were performed, and each qPCR reaction was run in three technical replicates. The primers used in this study are listed in Supplemental Table 3.

2.10. Enzyme-linked immunosorbent assay (ELISA)

The concentrations of chemokine (C−C motif) ligand 3 (CCL3), CCL4, CCL5, CCL19, C-X-C motif chemokine ligand 10 (CXCL10), CXCL12, and CXCL16 in mouse plasma were detected by an ELISA Kit (R&D Systems, Minneapolis, MN, USA) according to the manufacturer's protocols. For each cytokine, three biological replicates were performed, with independent samples from different animals.

2.11. Western blot

Cellular lysates were prepared using lysis buffer containing 1% Triton X-100, 1% sodium deoxycholate, 0.1% sodium dodecyl sulfate (SDS), supplemented with the protease inhibitor (catalog number: 36978; Thermo Fisher Scientific, Waltham, MA, USA) and the phosphatase inhibitor (catalog number: 4906837001; Sigma-Aldrich, St. Louis, MO, USA). Protein quantification was performed

with the Pierce™ BCA protein assay kit (catalog number: 23225; Thermo Fisher Scientific, Waltham, MA, USA). Protein samples (20 μg/lane) were electrophoresed through 10% sodium dodecyl sulfate-polyacrylamide gel electrophoresis (SDS-PAGE) gels and subsequently transferred to preactivated nitrocellulose membranes. The membranes were blocked with 5% skim milk and then incubated with primary antibodies at 4 °C overnight, followed by secondary antibodies for 1 h at room temperature. Finally, the protein signals were detected using the Amersham Imager 600 Imaging System (GE HealthCare Life Sciences, Chicago, IL, USA). For western blot analysis, a minimum of three biological replicates were carried out. The antibodies used in this study are listed in Supplemental Table 4.

2.12. Statistical analysis

Data are expressed as mean ± standard deviation (SD) from at least three independent experiments. Statistical analyses were performed using GraphPad Prism 8.3.0 (GraphPad Software, San Diego, CA, USA). Comparisons between the two groups were performed using the independent Student's *t*-test or Wilcoxon's test, depending on the data distribution. Survival curves were generated using the Kaplan-Meier method, and statistical differences between survival groups were evaluated using the Log-rank (Mantel-Cox) test. Tumor size comparisons were performed using two-way ANOVA. A *P*-value of <0.05 was considered statistically significant, and all statistical tests were two-sided.

3. Results

3.1. RFA combined with αPD-1 inhibits the growth of distant tumors

To investigate the abscopal effect of RFA combined with αPD-1 therapy, we established a bilateral subcutaneous HCC model. The right-flank tumors underwent complete RFA, while the left-flank tumors remained untreated. Mice were randomly divided into RFA or RFA+αPD-1 groups (Fig. 1A). Compared with monotherapy, the combination of RFA and αPD-1 therapy significantly reduced the weight and volume of the non-ablated left-flank tumors (Fig. 1B–C). Furthermore, mice receiving the combined treatment demonstrated prolonged survival (Fig. 1D). H&E staining revealed extensive necrosis in the non-ablated left-flank tumors following combination therapy (Fig. 1E). Moreover, no significant toxicity was observed in mice after combination therapy (Supplemental Fig. 1). These findings suggest that RFA synergizes with αPD-1 immunotherapy to suppress abscopal tumor growth and prolong the survival of HCC-bearing mice.

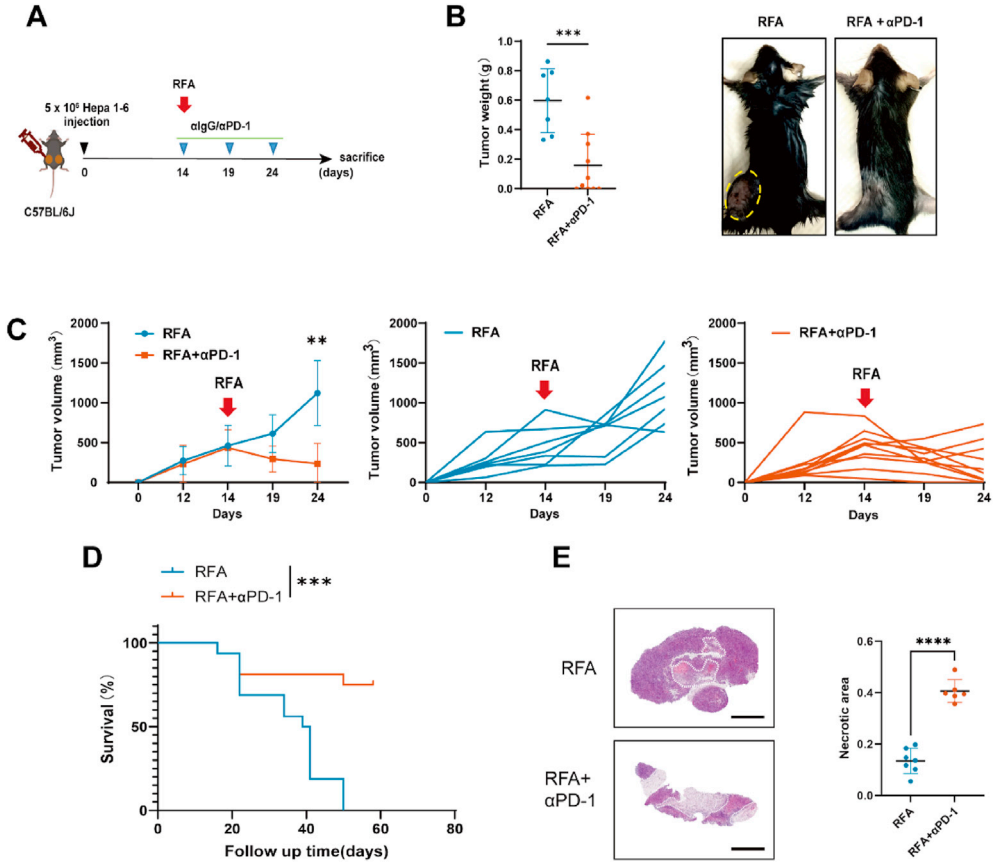

Fig. 1. RFA combined with αPD-1 suppresses non-ablated tumor growth and prolongs survival. (A) Schematic diagram of the experimental design. Mice were subcutaneously injected with Hepa 1–6 cells on both the right and left flank. Complete RFA treatment of the right-flank tumor was performed 2 weeks after tumor inoculation, when the tumor volume reached 500 mm^3. Mice were administered with αIgG/αPD-1 every 5 days respectively, for three doses. Blue markers indicate the time points of αIgG or αPD-1 antibody administration. All mice were sacrificed 1 day after the last treatment. **(B)** Left, tumor weight; right, representative gross images of mice treated with RFA ($n = 7$) and RFA+αPD-1 ($n = 10$). Yellow boxes highlight the subcutaneous tumor sites. **(C)** Tumor volume of non-ablated tumors in the RFA ($n = 7$) and RFA+αPD-1 groups ($n = 10$) at different time points. **(D)** Kaplan-Meier survival curves of the two treatment groups ($n = 16$ per group). **(E)** Representative H&E staining images of non-ablated tumors from the left flank in the RFA ($n = 7$) and RFA+ αPD-1 groups ($n = 6$). Necrotic areas are demarcated with white dashed lines. On the right, statistical analysis of the differences in necrotic areas between the two groups is shown. Data are presented as mean ± SD. $^{**}P < 0.01$; $^{***}P < 0.001$; $^{****}P < 0.0001$. Scale bar: 2 mm. Abbreviations: αPD-1, anti-programmed cell death protein 1; H&E, hematoxylin and eosin; RFA, radiofrequency ablation; SD, standard deviation.

3.2. RFA+αPD-1 shapes the immune microenvironment in distant tumors

It has been reported that RFA can induce systemic anti-tumor immune responses in various tumors.[16,17] However, research on the immune modulation of non-ablated distant tumors remains limited. Therefore, we further assessed the immune landscape of non-ablated left-flank tumors in the RFA monotherapy and RFA+αPD-1 groups using flow cytometry analysis (Supplemental Fig. 2A). We found that total $CD45^+$ immune cells were significantly increased in non-ablated left-flank tumors of the combination therapy group (Supplemental Fig. 3A), suggesting that local tumor ablation may trigger a significant immune response in abscopal tumors. The proportions of $CD3^+$ T cells and $CD8^+$ T cells were markedly higher in the combined treatment group, while $CD4^+$ T cells, B cells, natural killer (NK) cells, and macrophages were comparable between the two groups (Fig. 2A; Supplemental Fig. 3A). In addition, $CD11b^-CD11c^+$ DCs increased in the RFA+αPD-1 group (Fig. 2B–C). In contrast, total MDSCs and PMN-MDSCs were significantly reduced in the RFA+αPD-1 group (Fig. 2D–E). To assess the immunosuppressive function of PMN-MDSC, we isolated PMN-MDSCs from tumors of both the monotherapy and combination therapy groups and co-cultured them with CFSE-labeled splenic $CD8^+$ T cells at a 1:1 ratio. The results showed that the immunosuppressive ability of PMN-MDSCs to suppress $CD8^+$ T cell proliferation was decreased in the combined treatment group (Fig. 2F). Taken together, these data suggest that RFA combined with αPD-1 elicits an anti-tumor immune response in abscopal tumors.

3.3. RFA combined with aPD-1 increases $CD8^+$T cell and DC infiltration while reducing PMN-MDSCs in abscopal tumors

To further validate the infiltration and proportion of $CD8^+$ T cells and PMN-MDSCs in the non-ablated left-flank tumors, we conducted IHC staining for CD8, CD11b, and CD11c. We showed that, compared to the RFA monotherapy group, tumors in the combination therapy group exhibited increased infiltration of $CD8^+$ and $CD11c^+$ cells (Fig. 3A–B). Conversely, the expression of CD11b and Ly6G, which are markers commonly associated with PMN-MDSCs, was notably reduced (Fig. 3C–D). This shift in immune cell infiltration indicates that RFA combined with αPD-1 induces a favorable immune environment in the tumor microenvironment, particularly at abscopal, non-ablated tumor sites.

3.4. RFA+αPD-1 increases circulating T, B, and NK cells and reduces MDSCs in peripheral blood

To elucidate the impact of RFA combined with αPD-1 therapy on systemic immunity, we analyzed the dynamics of immune cells in peripheral blood and spleen by flow cytometry. Consistent with tumors, the proportions of $CD3^+$ T cells, $CD4^+$ T cells, and $CD8^+$ T cells in peripheral blood of the combination therapy group were notably increased compared to the RFA group, while the proportions of MDSCs and PMN-MDSCs were significantly decreased (Fig. 4A–D). Additionally, the combination therapy group also exhibited a significant increase in B cells and NK cells in peripheral blood (Supplemental Fig. 3B). However, there were no significant differences in the proportions of T cell subsets ($CD4^+$/$CD8^+$ T cells), DCs ($CD11c^+$), and MDSCs in the spleen between the two groups (Supplemental Fig. 3C). These data indicate that local RFA+αPD-1 therapy can induce systemic immune response with increased $CD3^+$, $CD4^+$, and $CD8^+$ T cells but decreased immunosuppressive PMN-MDSCs. However, its impact on the proportion of immune cells in the spleen was limited.

3.5. JAK-STAT1 activation and CXCL10 upregulation mediate the abscopal effect

To elucidate the molecular mechanism underlying the abscopal effect, we performed transcriptome sequencing on distant tumor tissues of the two groups. GSEA revealed that cytokine-cytokine receptor signaling, chemokine signaling, and Janus kinase-signal transducer and activator of transcription (JAK-STAT) signaling pathways were upregulated in the combined therapy group, whereas those related to ribosome and DNA replication were downregulated (Fig. 5A–C). Compared with the RFA group, 3567 genes were upregulated in the RFA+αPD-1 group, including 7 chemokines that were reported to be associated with T cell and DC chemotaxis (Fig. 5D). Furthermore, we detected the expression levels of these cytokines and chemokines in plasma and distant tumors from mice in both groups by ELISA and qPCR, respectively, and found that the CXCL10 concentration was significantly higher in the plasma and distant tumors of the RFA+αPD-1 group (Fig. 5E–F). Previous studies have demonstrated that STAT1 can directly bind to the interferon-stimulated response element in the promoter region of the *CXCL10* gene and initiate its transcription.[18–20] Given that RNA-sequencing indicated activation of the JAK-STAT signaling pathway in the combined treatment group, we further validated this finding by western blot. The results showed that STAT1 phosphorylation was upregulated in the distant tumor tissues of the combined therapy group (Fig. 5G–H). Taken together, these results suggest that RFA combined with αPD-1 therapy activates the JAK-STAT1 pathway in distant tumor tissues to upregulate CXCL10 expression, which attracts T cells and DCs into the tumor tissue, thereby inhibiting abscopal tumor growth.

3.6. RFA+αPD-1 induced durable immune memory against recurrent tumor

To investigate whether RFA+αPD-1 therapy could induce long-term immune memory to prevent tumor recurrence, we subcutaneously implanted HCC tumors on both flanks of the mice and performed RFA treatment with or without αPD-1. Then, we monitored tumor growth in the mice and found that 68.8% (11/16) of the mice in the RFA+αPD-1 group showed complete regression of both primary and distant tumors, wherea distant tumors in 100% (16/16) of the mice in the RFA group were not cured (Fig. 6A–C). Next, we reimplanted HCC tumors into the 11 mice that had been completely cured by RFA+αPD-1 at 56 days after tumor inoculation, and 25 days after rechallenge, all mice were sacrificed to collect blood for further analysis. The proportion of immune cells in peripheral blood was detected by flow cytometry. Interestingly, the rechallenge tumors were completely inhibited in these mice (Fig. 6B). After rechallenge, the proportions of total $CD4^+$ T cells, $CD8^+$ T cells, and central and effector memory $CD4^+$/$CD8^+$ T cells in the peripheral blood were significantly increased, indicating the activation of anti-tumor immune memory (Supplemental Fig. 2B, Fig. 6D–F). Taken together, RFA combined with αPD-1 therapy not only effectively suppresses primary tumors but also induces long-lasting immune memory to prevent the outgrowth of recurrent tumors.

4. Discussion

In this study, we found that the combination of RFA and PD-1 inhibition enhanced the abscopal effect to suppress non-ablated distant tumors, prolonged survival, and activated immune memory against recurrent tumors. Through flow cytometry, IHC staining, and RNA sequencing, we provided evidence of increased DCs and $CD8^+$T cells, reduced PMN-MDSC infiltration, and activation of

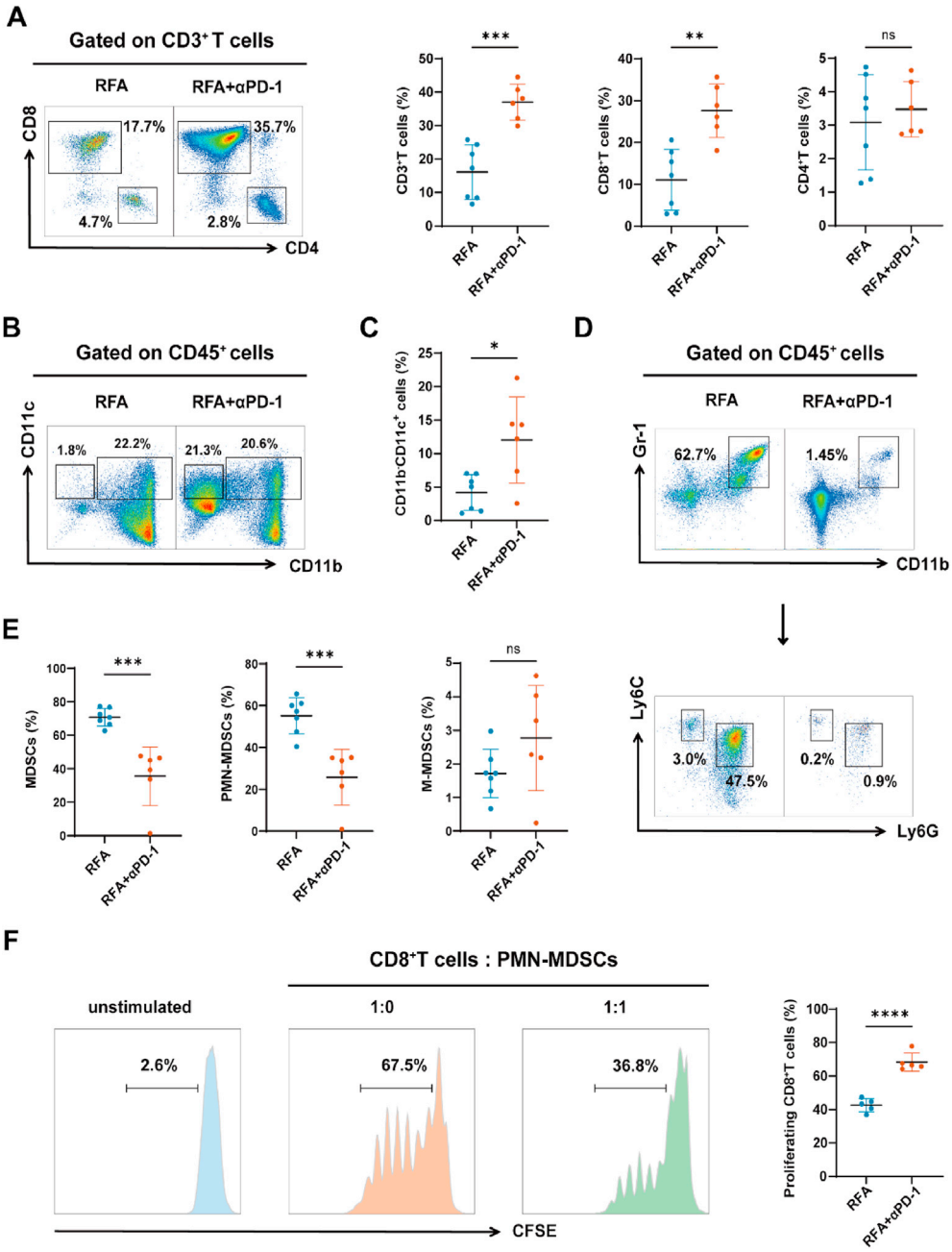

Fig. 2. Flow cytometric analysis of immune cell populations in distant (non-ablated) tumors. (A) Representative flow cytometry plots and percentages of $CD3^+$T cells, $CD8^+$T cells, and $CD4^+$T cells within $CD45^+$ cells. RFA, $n = 7$; RFA + anti-PD-1, $n = 6$. **(B)** Representative flow cytometry plots. **(C)** Percentages of $CD11b^-CD11c^+$ DCs within $CD45^+$ cells. RFA, $n = 7$; RFA + anti-PD-1, $n = 6$. **(D)** Representative flow cytometry plots. **(E)** Percentages of MDSCs, PMN-MDSCs, and M-MDSCs within $CD45^+$ cells. RFA, $n = 7$; RFA + anti-PD-1, $n = 6$. **(F)** PMN-MDSCs isolated from distant tumors of RFA and RFA+αPD-1 mice were co-cultured with CFSE-labeled splenic $CD8^+$ T cells at the ratio of 1:1 in the presence of CD3/CD28 and IL-2, and percentage of proliferating $CD8^+$T cells is shown ($n = 5$ per group). $^*P < 0.05$; $^{**}P < 0.01$; $^{***}P < 0.001$; $^{****}P < 0.0001$; ns, not significant. Abbreviations: αPD-1, anti-programmed cell death protein 1; CFSE, carboxyfluorescein succinimidyl ester; DCs, dendritic cells; IL-2, interleukin-2; Ly6G, lymphocyte antigen 6 complex locus G; M-MDSCs, monocytic myeloid-derived suppressor cells; MDSCs, myeloid-derived suppressor cells; PMN-MDSCs, polymorphonuclear myeloid-derived suppressor cells; RFA, radiofrequency ablation.

cytokine, chemokine, and JAK-STAT signaling pathways in the tumors of the combined treatment group, which was associated with tumor regression. In addition, the RFA+αPD-1 treatment induced durable immune memory against tumors, accompanied by an increase in total $CD4^+$T cells, $CD8^+$T cells, and central and effector memory T cells. Our study suggests that αPD-1 synergizes with RFA treatment to suppress abscopal tumors and activate immune memory to prevent tumor recurrence.

RFA is a minimally invasive therapeutic modality with a superior safety profile and has been widely used for early HCC. Compared with surgical resection, RFA treatment reduces the incidence of complications and shortens the hospitalization duration.[1] Emerging evidence suggests that RFA transiently activates anti-tumor immune responses through mechanisms involving immunogenic cell death — a process characterized by the release of damage-associated molecular patterns and subsequent presentation of

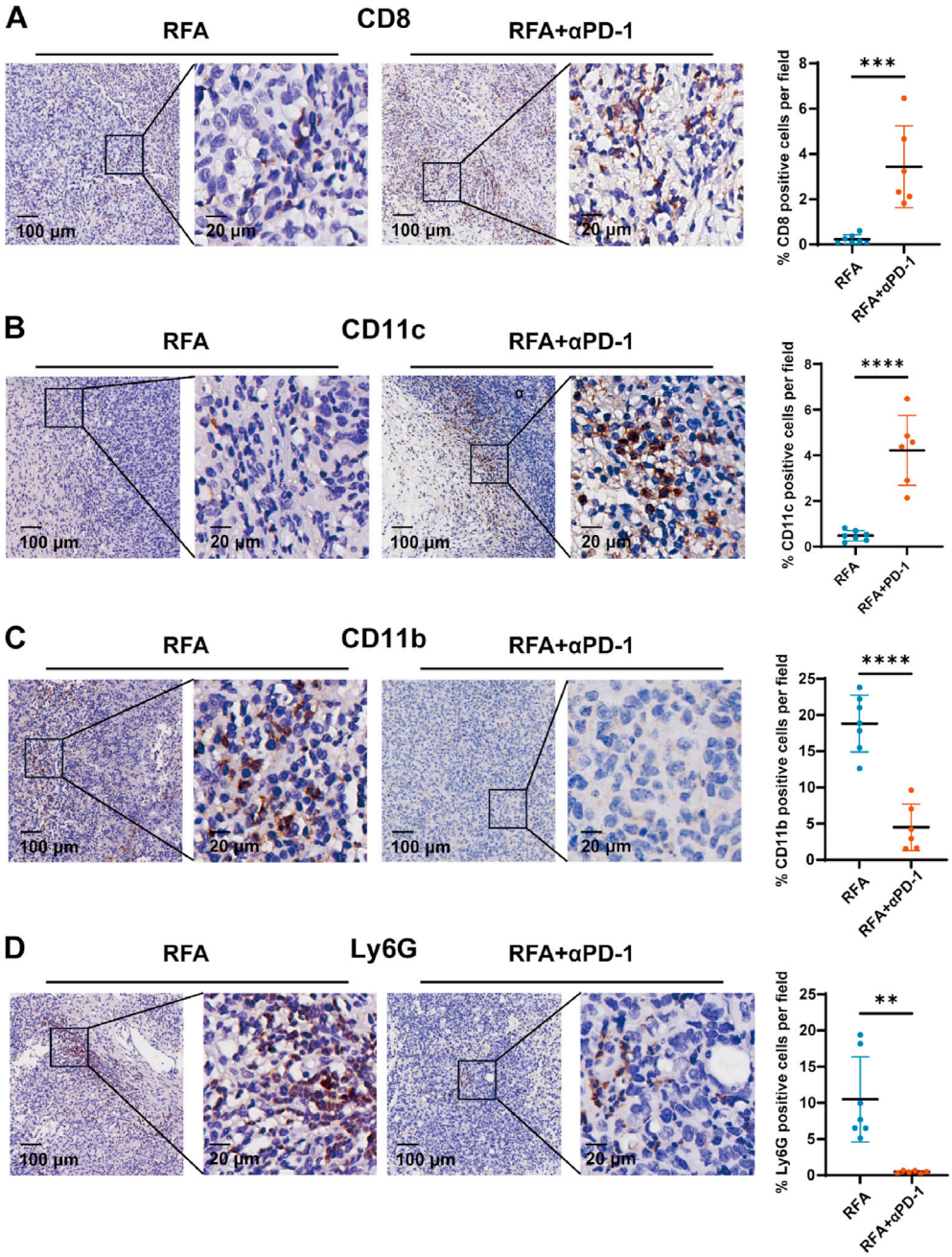

Fig. 3. Validation of CD8$^+$ T cell, DC, and PMN-MDSC infiltration in abscopal tumors by IHC staining. (A–D) IHC staining and statistical analysis of CD8 **(A)**, CD11c **(B)**, CD11b **(C)**, Ly6G **(D)** in abscopal tumors of RFA and RFA+αPD-1 group. RFA group, $n = 7$; RFA+αPD-1 group, $n = 6$. Scale bars: overview image = 100 μm; inset = 20 μm. $^{**}P < 0.01$; $^{***}P < 0.001$; $^{****}P < 0.0001$. Abbreviations: αPD-1, anti-programmed cell death protein 1; IHC, immunohistochemistry; Ly6G, lymphocyte antigen 6 complex locus G; MDSC, myeloid-derived suppressor cell; PMN-MDSC, polymorphonuclear myeloid-derived suppressor cell; RFA, radiofrequency ablation.

tumor antigens to elicit tumor-specific T cell responses.[21–23] However, Mizukoshi *et al.*[5] reported a paradoxical decline in cytotoxic T lymphocyte proportions within 87.5% of patients at the early post-ablation stage, indicating the transient nature of RFA-induced immune activation and its insufficiency to confer durable protection against tumor recurrence. To address this limitation, adjuvant therapeutic strategies have been explored to potentiate RFA efficacy. The phase III STORM trial (NCT00692770), a double-blind randomized controlled study, evaluated sorafenib administration following RFA or surgical resection versus placebo.[24] Unfortunately, this investigation failed to demonstrate a statistically significant improvement in recurrence-free survival, underscoring the complexity of achieving sustained therapeutic synergy between locoregional ablation and systemic molecular therapies.

Due to the immune-activating effects of RFA, several combined strategies have been explored. A retrospective clinical study observed that RFA combined with αPD-1 immunotherapy showed better efficacy than RFA alone in patients with recurrent HCC (1-year recurrence-free survival, 10.0% *vs.* 32.5%).[25] Preclinical studies also showed that the combination of RFA and αPD-1 can effectively extend survival and improve prognosis in mouse HCC models.[15,26] In our study, we observed no significant toxicity associated with the combination of RFA and αPD-1 therapy, which is consistent with findings from other studies on HCC and prostate cancer.[27,28]

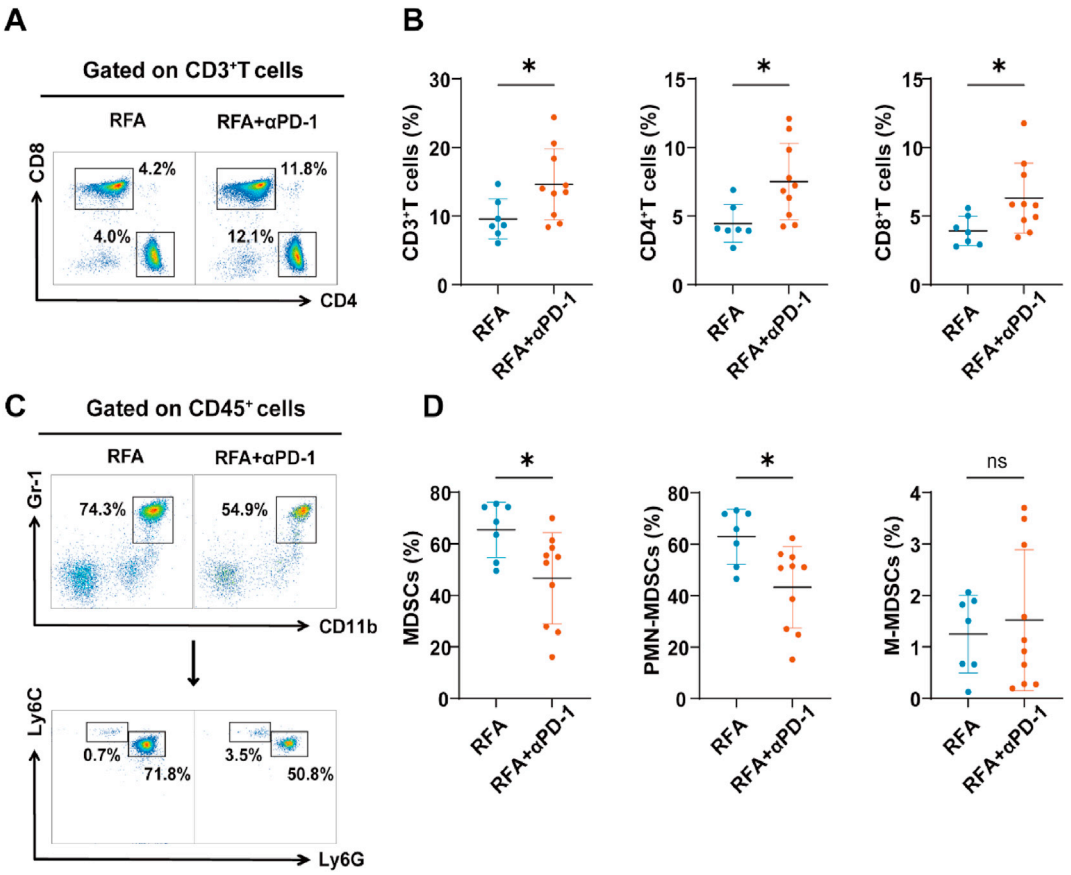

Fig. 4. Immune cell profiling of peripheral blood by flow cytometry. **(A)** Representative flow cytometry plots. **(B)** Percentages of $CD3^+$ T cells, $CD4^+$ T cells, and $CD8^+$ T cells in $CD45^+$ cells. **(C)** Representative flow cytometry plots. **(D)** Percentages of MDSCs, PMN-MDSCs, and M-MDSCs in $CD45^+$ cells. RFA, $n = 7$; RFA+αPD-1, $n = 10$. $^*P < 0.05$; ns, not significant. Abbreviations: αPD-1, anti-programmed cell death protein 1; Ly6G, lymphocyte antigen 6 complex locus G; M-MDSCs, monocytic myeloid-derived suppressor cells; MDSCs, myeloid-derived suppressor cells; PMN-MDSCs, polymorphonuclear myeloid-derived suppressor cells; RFA, radiofrequency ablation.

However, the underlying mechanisms remained incompletely understood. Although RFA has been reported to have an abscopal effect,[15,29] current research on HCC primarily focuses on the tumor on the RFA-treated side, with limited exploration of the distant tumors.[12] In our study, we found that, compared with RFA alone, the combination therapy effectively suppressed distant tumors and prolonged survival in mice, which is consistent with previous findings.[15] Consistent with tumor findings, increased $CD8^+$ T cells but decreased PMN-MDSCs were observed in peripheral blood, while there was no difference in immune cell infiltration in the spleen between the RFA and the combined treatment group. The discrepancy between the peripheral blood and spleen immune cell compositions may be due to the dynamic nature of immune cell activation and trafficking. Peripheral blood reflects circulating immune cells, which can be rapidly mobilized in response to systemic inflammation or antigen exposure, such as RFA-induced tumor necrosis and PD-1 blockade. In contrast, the spleen, a secondary lymphoid organ, may not show such acute fluctuations due to localized treatment. Additionally, the short observation period post-treatment might not allow for measurable changes in the splenic immune compartments. Further studies with additional time points and lymphoid tissue analyses are needed to better understand these spatial immunological dynamics.

It is well established that the tumor immune microenvironment is essential to tumor development, progression, and treatment response. The formation of the tumor microenvironment is influenced by various factors, including secreted factors from tumor cells, immune cell infiltration, and angiogenesis.[30] Previous studies have shown that RFA activates multiple signaling pathways, such as the heat shock protein 70 (HSP70) and proinflammatory cytokine pathways, which can alter immune cell functions and enhance tumor-specific T cell responses.[30–32] RFA significantly increases HSP70 expression in tumor tissues, which activates DCs and initiates anti-tumor immune responses. Furthermore, the necrosis induced by RFA releases immunogenic factors, including damage-associated molecular patterns like high mobility group box 1 (HMGB1), which activates antigen-presenting cells and promotes a more robust immune response, contributing to anti-tumor immunity.[31,33] In this study, by RNA sequencing analysis of abscopal tumor tissue, we found that the cytokine_cytokine_receptor_interaction, chemokine_signaling_pathway, and JAK_STAT_signaling_pathway were activated in the combined treatment group. The JAK-STAT signaling pathway is critically involved in the regulation of immune responses, cell proliferation, differentiation, and apoptosis. It is primarily activated by the binding of cytokines or growth factors to their respective receptors, which induces receptor dimerization or oligomerization. JAKs, associated with the intracellular domains of these receptors, undergo autophosphorylation and subsequently phosphorylate and activate STAT proteins. The phosphorylated STATs form dimers, translocate into the nucleus, and bind to specific DNA sequences to regulate the transcription of target genes.[34–36] Notably, the mRNA expression of chemokines such as CCL3, CCL4, CCL5, CCL19, CXCL10, CXCL12, and CXCL16 was upregulated. Previous studies reported that CCL3, CCL4, CCL5, and CCL19 can recruit

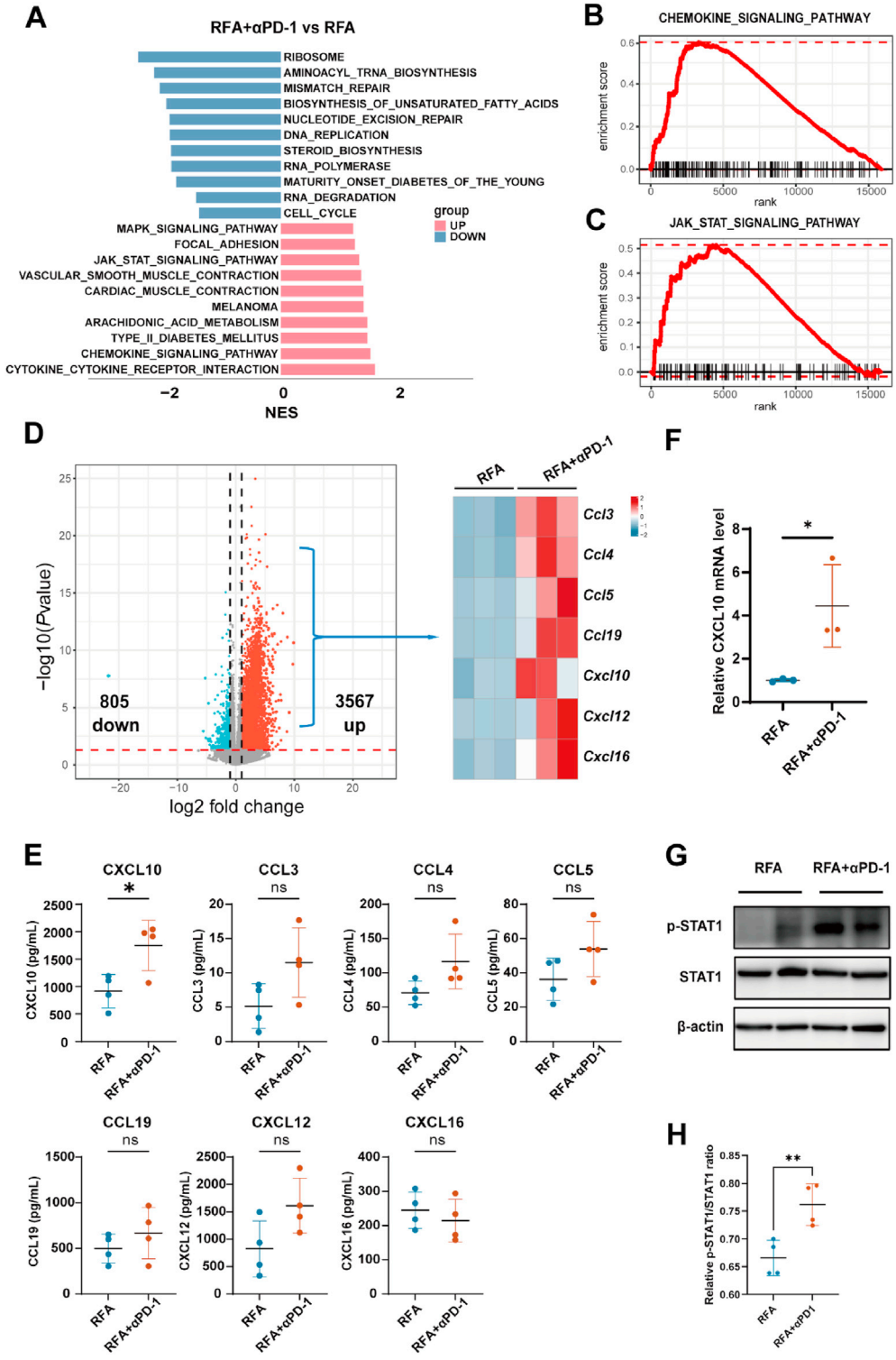

Fig. 5. Combined RFA and αPD-1 therapy activates JAK-STAT signaling and enhances CXCL10-mediated immune chemotaxis in abscopal tumors. **(A)** Differentially enriched pathways in abscopal tumors (RFA, $n = 3$; RFA+αPD-1, $n = 3$). **(B–C)** GSEA of the chemokine signaling pathway and the JAK-STAT signaling pathway. **(D)** Volcano plot showing DEGs between RFA and RFA+αPD-1 group. **(E)** CCL3, CCL4, CCL5, CCL19, CXCL10, CXCL12, and CXCL16 levels in mouse plasma were detected by ELISA (RFA, $n = 4$; RFA+αPD-1, $n = 4$). **(F)** qPCR analysis of *Cxcl10* mRNA in distant tumors of RFA and RFA+αPD-1 group, which were normalized to *Gapdh*. (RFA, $n = 3$; RFA+αPD-1, $n = 3$). **(G)** Western blot analysis of STAT1 and p-STAT1. β-actin was used as control. **(H)** Statistical analysis of p-STAT1/STAT1 ratio differences between RFA and RFA+αPD1 groups ($n = 4$). $^*P < 0.05$; $^{**}P < 0.01$; ns, not significant. Abbreviations: αPD-1, anti-programmed cell death protein 1; CCL3, chemokine (C–C motif) ligand 3; CXCL10, C-X-C motif chemokine ligand 10; DEGs, differentially expressed genes; ELISA, enzyme-linked immunosorbent assay; GSEA, gene set enrichment analysis; JAK-STAT, Janus kinase-signal transducer and activator of transcription; p-STAT1, phosphorylated signal transducer and activator of transcription 1; qPCR, quantitative polymerase chain reaction; RFA, radiofrequency ablation; STAT1, signal transducer and activator of transcription 1.

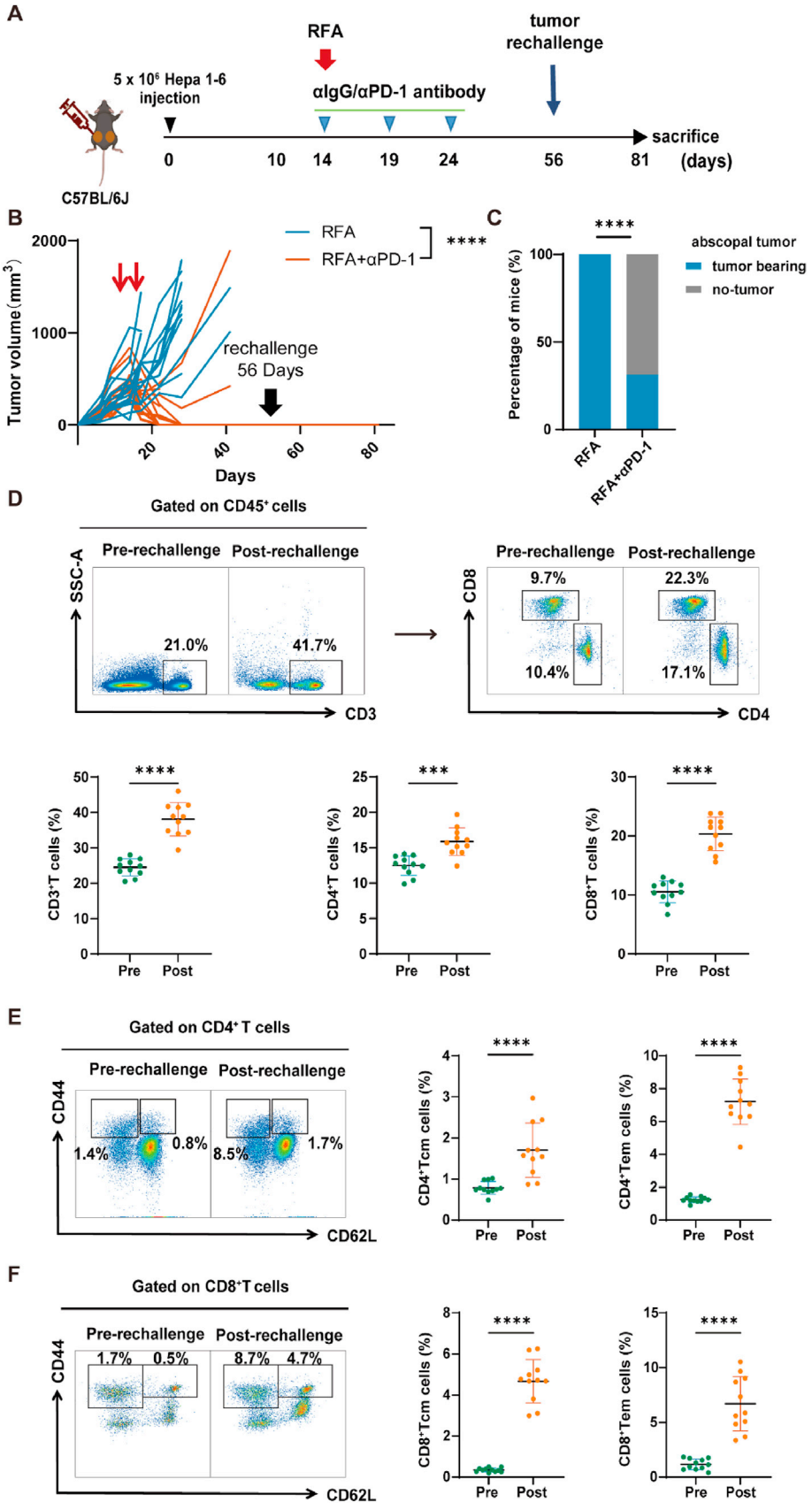

Fig. 6. RFA+αPD-1 therapy induces long-lasting immune memory to inhibit rechallenge tumors. (A) Schematic diagram of the *in vivo* tumor rechallenge experiment. C57BL/6J mice were subcutaneously injected with Hepa 1–6 cells on both flanks, followed by RFA treatment. αIgG or αPD-1 was injected every 5 days for 3 doses. Mice in the RFA + αPD-1 group that achieved complete tumor regression were rechallenged on day 56 with the same tumor cells. Mice were sacrificed 25 days after rechallenge. **(B)** Tumor volume of right-

flank tumors in RFA and RFA+αPD-1 mice at different time points (RFA, $n = 16$; RFA+αPD-1, $n = 16$). **(C)** The percentage of mice with or without abscopal tumors. **(D)** Representative flow cytometry plots and percentage of $CD3^+$T cells, $CD4^+$T cells, and $CD8^+$T cells in $CD45^+$ cells. $n = 11$. **(E)** Representative flow cytometry plots and percentages of $CD4^+$ central memory T cells and $CD4^+$ effector memory T cells in $CD45^+$ cells. $n = 11$. **(F)** Representative flow cytometry plots and percentages of $CD8^+$ central memory T cells and $CD8^+$ effector memory T cells in $CD45^+$ cells. $n = 11$. $^{***}P < 0.001$; $^{****}P < 0.0001$. Abbreviations: αIgG, anti-immunoglobulin G; αPD-1, anti-programmed cell death protein 1; Pre, pre-rechallenge; Post, post-rechallenge; RFA, radiofrequency ablation; Tcm, central memory T cell; Tem, effector memory T cell.

$CD4^+$ and $CD8^+$ T cells, as well as DCs, to the tumor site, thereby enhancing their anti-tumor effects.[37–39] CXCL10 and CXCL12 can promote the directional migration and functional activation of immune cells within the tumor microenvironment.[37–39] Using ELISA to detect these chemokines, we validated that CXCL10, a proinflammatory chemokine that promotes recruitment of $CD8^+$ effector and $CD4^+$ T cells, was upregulated in peripheral blood of the RFA+αPD-1 group. In addition, the JAK-STAT signaling pathway was activated in the abscopal tumor of the combined treatment group by western blot. Overall, the combination therapy modulates the tumor immune microenvironment by activating the JAK-STAT pathway and upregulating CXCL10 expression to recruit effector T cells for anti-tumor immunity.

Immune responses against cancer rely on T cells that are specific to cancer-related antigens. Immune memory plays a critical role in providing long-term protection against tumor recurrence, thus offering prolonged protection to the host.[40] Here, we showed that PD-1 blockade synergized with RFA treatment to induce immune memory, and remarkably inhibited outgrowth of rechallenge tumor. The total number of $CD4^+$, $CD8^+$ T cells, and central and effector memory T cells in blood was significantly increased after tumor rechallenge.

However, this study has several limitations. First, the subcutaneous tumor model may not fully recapitulate the immunobiology of orthotopic or spontaneous liver tumors. Second, only one HCC cell line (Hepa 1–6) was employed; further validation in other syngeneic or patient-derived models is warranted. Finally, the efficacy of RFA+αPD-1 in HCC awaits further investigation in clinical trials.

5. Conclusions

This study found that compared with RFA monotherapy, the combination of RFA and αPD-1 significantly suppressed abscopal tumors by activating the JAK-STAT pathway to recruit cytotoxic T cells. In addition, the combined treatment activated immune memory to inhibit rechallenge tumors. The combination of RFA and αPD-1 may be a potential therapeutic strategy for HCC patients with a high risk of recurrence, but awaits further investigation in clinical trials.

Authors' contributions

Kai Lei: Writing – original draft, Validation, Project administration, Methodology, Investigation, Formal analysis, Data curation, Conceptualization. **Shuang Li:** Writing – original draft, Validation, Methodology, Investigation, Formal analysis, Data curation. **Jiale Chen:** Validation, Methodology, Investigation. **Zebin Chen:** Writing – review & editing, Supervision. **Fang Wang:** Writing – review & editing, Supervision. **Xuezhen Zeng:** Writing – review & editing, Supervision, Project administration, Methodology, Investigation, Funding acquisition, Conceptualization.

Data availability statement

The data contained in this manuscript or supplementary material will be made available upon request from the corresponding author.

Declaration of competing interest

The authors declare that they have no conflict of interest.

Acknowledgements

This study is funded by the National Natural Science Foundation of China to Xuezhen Zeng (No. 82372777) and the Kelin Foundation for Distinguished Young Scholars to Xuezhen Zeng (No. R07014).

Appendix A. Supplementary data

Supplementary data to this article can be found online at https://doi.org/10.1016/j.livres.2025.05.003.

References

1. Vogel A, Meyer T, Sapisochin G, Salem R, Saborowski A. Hepatocellular carcinoma. *Lancet*. 2022;400:1345–1362. https://doi.org/10.1016/S0140-6736(22)01200-4.
2. Siegel RL, Miller KD, Wagle NS, Jemal A. Cancer statistics, 2023. *CA Cancer J Clin*. 2023;73:17–48. https://doi.org/10.3322/caac.21763.
3. Wang H, Wu Z, Cui D, Shi Y, Zhai B. Radiofrequency ablation of hepatocellular carcinoma: current status, challenges, and prospects. *Liver Res*. 2023;7:108–115. https://doi.org/10.1016/j.livres.2023.05.002.
4. Heimbach JK, Kulik LM, Finn RS, et al. AASLD guidelines for the treatment of hepatocellular carcinoma. *Hepatology*. 2018;67:358–380. https://doi.org/10.1002/hep.29086.
5. Mizukoshi E, Yamashita T, Arai K, et al. Enhancement of tumor-associated antigen-specific T cell responses by radiofrequency ablation of hepatocellular carcinoma. *Hepatology*. 2013;57:1448–1457. https://doi.org/10.1002/hep.26153.
6. Shi L, Wang J, Ding N, et al. Inflammation induced by incomplete radiofrequency ablation accelerates tumor progression and hinders PD-1 immunotherapy. *Nat Commun*. 2019;10:5421. https://doi.org/10.1038/s41467-019-13204-3.
7. Liu X, Zhang W, Xu Y, et al. Targeting PI3Kgamma/AKT pathway remodels LC3-Associated phagocytosis induced immunosuppression after radiofrequency ablation. *Adv Sci (Weinh)*. 2022;9:e2102182. https://doi.org/10.1002/advs.202102182.
8. Ali MY, Grimm CF, Ritter M, et al. Activation of dendritic cells by local ablation of hepatocellular carcinoma. *J Hepatol*. 2005;43:817–822. https://doi.org/10.1016/j.jhep.2005.04.016.
9. Erinjeri JP, Thomas CT, Samoilia A, et al. Image-guided thermal ablation of tumors increases the plasma level of interleukin-6 and interleukin-10. *J Vasc Interv Radiol*. 2013;24:1105–1112. https://doi.org/10.1016/j.jvir.2013.02.015.
10. Ngwa W, Irabor OC, Schoenfeld JD, et al. Using immunotherapy to boost the abscopal effect. *Nat Rev Cancer*. 2018;18:313–322. https://doi.org/10.1038/nrc.2018.6.
11. Yousaf MN, Ehsan H, Muneeb A, et al. Role of radiofrequency ablation in the management of unresectable pancreatic cancer. *Front Med (Lausanne)*. 2020;7:624997. https://doi.org/10.3389/fmed.2020.624997.
12. Zeng X, Liao G, Li S, et al. Eliminating METTL1-mediated accumulation of PMN-MDSCs prevents hepatocellular carcinoma recurrence after radiofrequency ablation. *Hepatology*. 2023;77:1122–1138. https://doi.org/10.1002/hep.32585.
13. Fei Q, Pan Y, Lin W, et al. High-dimensional single-cell analysis delineates radiofrequency ablation induced immune microenvironmental remodeling in pancreatic cancer. *Cell Death Dis*. 2020;11:589. https://doi.org/10.1038/s41419-020-02787-1.
14. Yi M, Zheng X, Niu M, et al. Combination strategies with PD-1/PD-L1 blockade: current advances and future directions. *Mol Cancer*. 2022;21:28. https://doi.org/10.1186/s12943-021-01489-2.
15. Sun T, Sun B, Cao Y, et al. Synergistic effect of OK-432 in combination with an anti-PD-1 antibody for residual tumors after radiofrequency ablation of hepatocellular carcinoma. *Biomed Pharmacother*. 2023;166:115351. https://doi.org/10.1016/j.biopha.2023.115351.
16. Napoletano C, Taurino F, Biffoni M, et al. RFA strongly modulates the immune system and anti-tumor immune responses in metastatic liver patients. *Int J Oncol*. 2008;32:481–490.
17. Hirata T, Sugimoto K, Soya R, et al. Comparative analysis of systemic immune responses and metastatic risks in tumor ablation: an animal study of radiofrequency ablation and irreversible electroporation with immune modulation.

Cardiovasc Interv Radiol. 2025;48:524–535. https://doi.org/10.1007/s00270-024-03938-z.
18. Hiroi M, Ohmori Y. Constitutive nuclear factor kappaB activity is required to elicit interferon-gamma-induced expression of chemokine CXC ligand 9 (CXCL9) and CXCL10 in human tumour cell lines. *Biochem J*. 2003;376:393–402. https://doi.org/10.1042/BJ20030842.
19. Clarke DL, Clifford RL, Jindarat S, et al. TNFalpha and IFNgamma synergistically enhance transcriptional activation of CXCL10 in human airway smooth muscle cells via STAT-1, NF-kappaB, and the transcriptional coactivator CREB-binding protein. *J Biol Chem*. 2010;285:29101–29110. https://doi.org/10.1074/jbc.M109.0999952.
20. Au KK, Le Page C, Ren R, et al. STAT1-associated intratumoural T(H)1 immunity predicts chemotherapy resistance in high-grade serous ovarian cancer. *J Pathol Clin Res*. 2016;2:259–270. https://doi.org/10.1002/cjp2.55.
21. Minami Y, Nishida N, Kudo M. Radiofrequency ablation of liver metastasis: potential impact on immune checkpoint inhibitor therapy. *Eur Radiol*. 2019;29:5045–5051. https://doi.org/10.1007/s00330-019-06189-6.
22. Shi L, Chen L, Wu C, et al. PD-1 blockade boosts radiofrequency ablation-elicited adaptive immune responses against tumor. *Clin Cancer Res*. 2016;22:1173–1184. https://doi.org/10.1158/1078-0432.CCR-15-1352.
23. Takahashi Y, Matsutani N, Nakayama T, et al. Immunological effect of local ablation combined with immunotherapy on solid malignancies. *Chin J Cancer*. 2017;36:49. https://doi.org/10.1186/s40880-017-0216-5.
24. Bruix J, Takayama T, Mazzaferro V, et al. Adjuvant sorafenib for hepatocellular carcinoma after resection or ablation (STORM): a phase 3, randomised, double-blind, placebo-controlled trial. *Lancet Oncol*. 2015;16:1344–1354. https://doi.org/10.1016/S1470-2045(15)00198-9.
25. Wang X, Liu G, Chen S, et al. Combination therapy with PD-1 blockade and radiofrequency ablation for recurrent hepatocellular carcinoma: a propensity score matching analysis. *Int J Hyperther*. 2021;38:1519–1528. https://doi.org/10.1080/02656736.2021.1991011.
26. Zhang S, Huang Y, Pi S, et al. Autophagy-amplifying nanoparticles evoke immunogenic cell death combined with anti-PD-1/PD-L1 for residual tumors immunotherapy after RFA. *J Nanobiotechnol*. 2023;21:360. https://doi.org/10.1186/s12951-023-02067-y.
27. Chen S, Liu R, Duan S, et al. Ultrasound-guided percutaneous radiofrequency ablation combined with anti-PD-1 for the treatment of prostate cancer: an experimental study. *Front Oncol*. 2025;15:1527763. https://doi.org/10.3389/fonc.2025.1527763.
28. Xiao T, Hu S, Dong S, et al. A study on combination of non-ablative local RFA with PD-1 and angiogenesis blocking to prolong survival through improvement of immune microenvironment in advanced hepatocellular carcinoma. *Int Immunopharmacol*. 2024;134:112144. https://doi.org/10.1016/j.intimp.2024.112144.
29. Faraoni EY, O'Brien BJ, Strickland LN, et al. Radiofrequency ablation remodels the tumor microenvironment and promotes neutrophil-mediated abscopal immunomodulation in pancreatic cancer. *Cancer Immunol Res*. 2023;11:4–12. https://doi.org/10.1158/2326-6066.CIR-22-0379.
30. Chu KF, Dupuy DE. Thermal ablation of tumours: biological mechanisms and advances in therapy. *Nat Rev Cancer*. 2014;14:199–208. https://doi.org/10.1038/nrc3672.
31. Sabel MS. Cryo-immunology: a review of the literature and proposed mechanisms for stimulatory versus suppressive immune responses. *Cryobiology*. 2009;58:1–11. https://doi.org/10.1016/j.cryobiol.2008.10.126.
32. Teng L, Jin K, Han N, Cao J. Radiofrequency ablation, heat shock protein 70 and potential anti-tumor immunity in hepatic and pancreatic cancers: a minireview. *Hepatobiliary Pancreat Dis Int*. 2010;9:361–365.
33. den Brok MHMG, Sutmuller RPM, van der Voort R, et al. In situ tumor ablation creates an antigen source for the generation of antitumor immunity. *Cancer Res*. 2004;64:4024–4029. https://doi.org/10.1158/0008-5472.CAN-03-3949.
34. Philips RL, Wang Y, Cheon H, et al. The JAK-STAT pathway at 30: much learned, much more to do. *Cell*. 2022;185:3857–3876. https://doi.org/10.1016/j.cell.2022.09.023.
35. Wang J, Zhang Y, Song H, et al. The circular RNA circSPARC enhances the migration and proliferation of colorectal cancer by regulating the JAK/STAT pathway. *Mol Cancer*. 2021;20:81. https://doi.org/10.1186/s12943-021-01375-x.
36. de Bock CE, Demeyer S, Degryse S, et al. HOXA9 cooperates with activated JAK/STAT signaling to drive leukemia development. *Cancer Discov*. 2018;8:616–631. https://doi.org/10.1158/2159-8290.CD-17-0583.
37. Wang H, Wang T, Yan S, et al. Crosstalk of pyroptosis and cytokine in the tumor microenvironment: from mechanisms to clinical implication. *Mol Cancer*. 2024;23:268. https://doi.org/10.1186/s12943-024-02183-9.
38. Waldmann TA. Cytokines in cancer immunotherapy. *Cold Spring Harbor Perspect Biol*. 2018;10. https://doi.org/10.1101/cshperspect.a028472.
39. Propper DJ, Balkwill FR. Harnessing cytokines and chemokines for cancer therapy. *Nat Rev Clin Oncol*. 2022;19:237–253. https://doi.org/10.1038/s41571-021-00588-9.
40. Chen DS, Mellman I. Elements of cancer immunity and the cancer-immune set point. *Nature*. 2017;541:321–330. https://doi.org/10.1038/nature21349.